Desalination and Water Treatment
www.deswater.com

34 (2011) 277–283
October

1944-3994/1944-3986
doi: 10/5004/dwt.2011.2802

Permeability calculation of sphere-packed porous media using dissipative particle dynamics

Yong Shi[a], Yong Taek Lee[b], Albert S. Kim[a,b,*]

[a]*Department of Civil and Environmental Engineering, University of Hawaii at Manoa, 2540 Dole Street Holmes 383, Honolulu, Hawaii 96822, USA*
[b]*Department of Chemical Engineering, College of Engineering, Kyung Hee University, Gyeonggi-do 4460701, Korea*
Tel. +1 (808) 956-3718; email: albertsk@hawaii.edu

Received 3 September 2010; Accepted 3 January 2011

ABSTRACT

In this study we developed a fundamental method to directly calculate hydraulic permeability and tortuosity relative to the Happel cell model [AIChE J. 4 (1958) 197–201] without any macroscopic assumptions. No transparent structural dependence was observed in hydraulic permeabilities from simulation results of parallel dissipative hydrodynamics. The Happel cell model constantly underestimates, by a minimum of volume fraction 0.524, the permeability of sphere-packed porous media using simple cubic, body-centered cubic, face-centered cubic, and random cake structures. Accurate uses of the Happel cell model and Carman-Kozeny equation are limited to a narrow range of dense volume fractions from 0.524 to 0.64, above which the true depiction of the permeability from dissipative particle dynamics (DHD) provides lower permeability than that estimated using conventional theories.

Keywords: Hydraulic permeability; Hydraulic tortuosity; Random packing structures; Solid state structures; Stokesian dynamics; Dissipative hydrodynamics

1. Introduction

Water permeation through porous media is a ubiquitous phenomenon in natural and engineered processes, including membrane filtration. When particulates are rejected on membrane surfaces, a cake layer forms and provides significant hydraulic resistance. If the particle sintering method is used to prepare microfiltration or ultrafiltration membranes, water transport through sphere-packed porous media (i.e., membranes) is fundamentally similar to the transport through cake layers [1]. In addition, the role of the porous support layer in pressure-retarded osmosis and forward osmosis is of interest due to its hindrance of solute diffusion as well as resistance to water permeation [2]. Research on permeability of a sphere-swarm is still in a burgeoning state because rigorous microscopic simulation tools are mathematically complex and computationally very intensive. For accurate estimation of permeability, hydrodynamic forces exerted on particles should be precisely calculated using the particle sizes, volume fraction, and internal configuration of the sphere-packed porous media. The pressure gradient across the porous media is equivalent to the hydrodynamic force density and is inversely proportional to the permeability. Therefore, structural dependence of the permeability can be characterized using hydrodynamic tortuosity if the drag forces are accurately calculated [3,4].

In this study, we calculated hydraulic permeabilities of various models of porous media composed of mono-dispersed spheres such as simple cubic (SC), body-centered-cubic (BCC), face-centered-cubic (FCC),

*Corresponding author.

Presented at the AMS6/IMSTEC10, The 6th conference of the Aseanian Membrane Society in conjunction with the 7th International Membrane Science and Technology Conference, Sydney, Australia, November 22–26, 2010

and random cake (RC) structures [5–7]. Hydrodynamic forces and torques exerted on particles forming these well-characterized structures are calculated using the recently developed dissipative particle dynamics (DHD) [8]. *N* equal-sized spherical particles are located in a uniform up-flow, and the grand mobility matrix was built based on the relative particle positions. Then, drag forces in the fluid flow direction were calculated using the parallel *LU* decomposition technique. As many as 10,000 particles were simulated to estimate the hydraulic permeability and tortuosity, of which the grand mobility tensor has matrix elements on the order of billions. This huge linear system was solved using ScaLAPACK library for parallel computations [9]. We found that the random internal structure of the sphere-packed porous medium has noticeable influence on the permeability; and permeability models provide reasonable approximations only for closely packed structures of volume fraction around the random loose packing (RLP) ratio of 0.60 [10].

2. Simulation method

2.1. Generation of porous media structures

As stated above, we selected four model structures of sphere-packed porous media, i.e., SC, BCC, FCC and RC. A unit cell of SC structure consists of eight spheres positioned at each corner of a cube. BCC structures have one more sphere in the center of the SC cube and FCC structures have six additional spheres on each face of the SC cube. The net number of spheres in SC, BCC, and FCC cells are 1 ($= 8 \times \frac{1}{8}$), 2($= 8 \times \frac{1}{8} + 1$), and 4 ($= 8 \times \frac{1}{8} + 6 \times \frac{1}{2}$), respectively, because spheres at a corner contribute one eighth of a sphere volume and spheres on a face contribute a half of a sphere volume. The RC structure is obtained by using a simple Monte Carlo technique for hard spheres [11]. Each particle moves randomly with a displacement much smaller than the distance to the nearest neighbor. If the particle at a new proposed position overlaps with any other particles, it returns to the original position; otherwise, it stays at the new location and the next random movement is executed. Since condensation from a dilute configuration to a dense random packing structure is not a simple task, we reversed the process as this is known to be more effective. We started with a FCC structure of volume fraction 0.70 and shook the particle system to generate a random structure using the Monte Carlo algorithm described above. For RC structures of lower volume fractions, we changed the particle coordinate from the center of mass position to increase the porosity and performed extra Monte Carlo movements to enhance the structural randomness and remove any correlation from the parent structure.

Once each structure with a number of particles $N = O(10^3–10^4)$ is generated in a cubic box of each length *L*, we removed particles near the edges if their distances from the center of the box were larger than the half length. The remaining particles are within a spherical shell of radius 0.5 *L* and form a spherical swarm. The number of particles forming a spherical swarm is less than that of a large cubic array. We developed a simple algorithm that suggests *n* primary spheres of a spherical swarm, which eventually consists of *N* spheres quite close to the proposed *n*. The characteristic radius of the spherical swarm is estimated to be the outer radius based on the gyration radius. See section 2.3 for details.

2.2. Calculation of generalized hydrodynamic forces

Bossis and Brady [12] developed a computationally intensive method called Stokesian dynamics for numerically simulating dynamics of interacting spherical particles, of which the hydrodynamic force calculation is identical to that of DHD. For a small particle Reynolds number, the hydrodynamic force/torque *F* of dimension 6*N* exerted on *N* stationary particles in a uniform flow is described as

$$U^{\infty} = M^{\infty} \cdot F^{\infty} \tag{1}$$

where $M^{\bullet}$ is the far-field mobility matrix of dimension $6N \times 6N$. Since the ambient up-flow to each particle is expressed as $U^{\bullet} = (0, 0, +1, 0, 0, 0)$ in a dimensionless form, *F* is calculated using the standard parallel *LU* decomposition method after the grand mobility matrix is set up using relative coordinates for *N* particles. When particles move in a concentrated suspension with averaged surface-to-surface distances ranging in length from their radii or smaller, lubrication forces play an important role in near-field hydrodynamic repulsion. In that case, $M^{\bullet}$ needs to be inverted and updated with the difference between exact near-field lubrication forces and approximate many-body far-field hydrodynamic forces between two particles [12]. However, when particles are fixed in space without performing relative motions or their relative distances are constrained, the lubrication forces overestimate the near-field hydrodynamics interactions, leaving the far-field grand mobility as an excellent link between generalized forces and velocities for non-touching spherical particles [13].

2.3. Calculation of hydraulic permeability

Hydraulic permeability is, by definition, a quantity to measure the ability of a porous material of specific internal geometry to transmit a fluid of viscosity μ, and is independent of the nature of the fluid flow.

For creeping flow through an isotropic porous medium, Darcy's law defines the (intrinsic) permeability κ as

$$u = -\frac{\kappa}{\mu}\nabla P \tag{2}$$

where u is the superficial fluid velocity through the medium, μ the fluid viscosity, and P the pressure. For particle swarms composed of primary particles of radius a, the dimensionless permeability, defined as κ/a^2, strongly depends on the solid volume fraction of the media ϕ. This dependence can vary with the internal structure of the media in a way that is difficult to predict from the first principles. Various investigators developed the permeability expressions for porous media. Due to its simplicity and elegance, the Happel cell model [14] is regarded as an excellent tool for predicting permeability of packed beds consisting of identical spheres:

$$\kappa_{\text{Happel}} = \left(\frac{2a^2}{9\phi}\right)\left[\frac{6 - 9\phi^{1/3} + 9\phi^{5/3} - 6\phi^2}{6 + 4\phi^{5/3}}\right] \tag{3}$$

which in the dilute limit reduces to [15]

$$\kappa_{\text{DL}} = \frac{2a^2}{9\phi} \tag{4}$$

On the other hand, the Carman-Kozeny (CK) equation [16] is a widely used, semi-empirical expression for permeability of a dense sphere-packed swarm:

$$\kappa_{\text{CK}} = \left(\frac{2a^2}{9\phi}\right)\left[\frac{(1-\phi)^3}{2c\phi}\right] \tag{5}$$

where c is a parameter, empirically obtained as 5. Although these models provide good insight on how the permeability changes with volume fraction, influence of the internal geometry on the macroscopic permeability is also an important issue.

Stokes' law expresses the drag force exerted on an impermeable rigid sphere of radius R, experiencing relative velocity U, as

$$\boldsymbol{F}_{\text{Stokes}} = 6\pi\mu RU \tag{6}$$

and another system of great interest is a uniformly porous, spherical aggregate of the same radius R, held fixed in a unidirectional fluid flow or sinking in a motionless fluid with velocity U. Brinkman [17] developed a solution for the drag force acting on the uniformly porous sphere, on which the stresses and velocities were considered to be continuous. An effective viscosity within the porous sphere was assumed to be identical to that of the bulk phase. A dimensionless parameter, defined as

$$\beta = \frac{R}{\sqrt{\kappa}} \tag{7}$$

represents the ratio of the (characteristic) radius of the porous sphere to the penetration depth of the fluid flow (from the surface to the center of the porous sphere) estimated as $\sqrt{\kappa}$ [18]. The hydrodynamic force F exerted on the porous sphere by the uniform flow can be scaled using Stokes' law:

$$\boldsymbol{F} = \Omega\boldsymbol{F}_{\text{Stokes}} \tag{8}$$

where

$$\Omega(\beta) = \frac{2\beta^2(1 - \tanh\beta/\beta)}{2\beta^2 + 3(1 - \tanh\beta/\beta)} \le 1 \tag{9}$$

is a correction factor, indicating that the permeableness of the porous sphere reduces the drag force from Stokes' drag by allowing the fluid to partially penetrate the porous sphere. Ω can be also regarded as the ratio of the settling velocity of a solid sphere to that of a permeable sphere of the same size and total solid mass.

If N primary particles of radius a form a spherical assemblage of radius R, then the drag force acting on each particle can be calculated using Eq. (1) and the correction factor is

$$\Omega = \frac{F}{F_{\text{Stokes}}} = \frac{a}{R}\sum_{i=1}^{N} f_i \tag{10}$$

where $f_i(\le 1)$ is the dimensionless hydrodynamic force in the flow direction acting on the ith particle, i.e., the drag force on the ith particle in the swarm divided by that when isolated. The gyration radius of the N-sphere swarm is calculated as

$$R_g^2 = \frac{1}{N}\sum_{i}^{N}\left(\vec{r}_i - \vec{r}_{CM}\right)^2 \tag{11}$$

where $\vec{r}_i$ and $\vec{r}_{\text{CM}}$ are positions of the ith particle and the center-of-mass of the N particles. The outer radius R of the assemblage is defined in terms of the gyration radius R_g as

$$R = \sqrt{\frac{5}{3}}R_g \tag{12}$$

and, finally, the volume fraction of the sphere-packed porous media is calculated as

$$\phi = N\left(\frac{a}{R}\right)^2 \tag{13}$$

The overall procedure of the permeability calculation using the DHD simulation method and Brinkman theory is as follows:

i. forces and torques exerted on each particle are calculated using Eq. (1),
ii. the correction factor Ω is determined using Eq. (10),
iii. β is numerically calculated using Eq. (9) with Ω calculated in step (ii), and the outer radius calculated using Eq. (12), and finally
iv. permeability κ is calculated using Eq. (7) and plotted with respect to ϕ of Eq. (13).

When the porous medium is densely packed with a high volume fraction, the permeability decreases to a negligible value, providing a large value of β followed by Ω converging to 1.0. Therefore, it should be noted that inverse estimation of β using Eq. (9) is very sensitive to accurate calculation of Ω as well as the outer radius *R*, especially for dense structures.

3. Results and discussions

3.1. Permeability ratio

Hydraulic permeabilities of SC, BCC, FCC and RC structures were investigated as a function of the volume fraction, and those scaled by the Happel cell model, i.e., permeability ratio, are shown in Fig. 1. The inaccuracy of the CK equation based on the hydraulic diameter at low volume fractions led us to select the Happel model as our reference permeability [16]. The accuracy of mean-field approximations of permeability theories are compared to and analyzed with the rigorous and accurate DHD simulation results.

SC structure. Variation of the permeability ratio of the SC porous medium is shown in Fig. 1(a). Volume fraction increases from 0.01 to the maximum packing ratio (MPR) π/6 (= 0.524) where each particle touches six nearest neighbors. The number of particles seems to influence the permeability ratio, but no specific trend is clearly observed. In general, the reliability of simulation increases with the number of particles. Convergence of the permeability ratio to 1.0 at low volume fractions, especially ϕ smaller than 0.1, validates the DHD

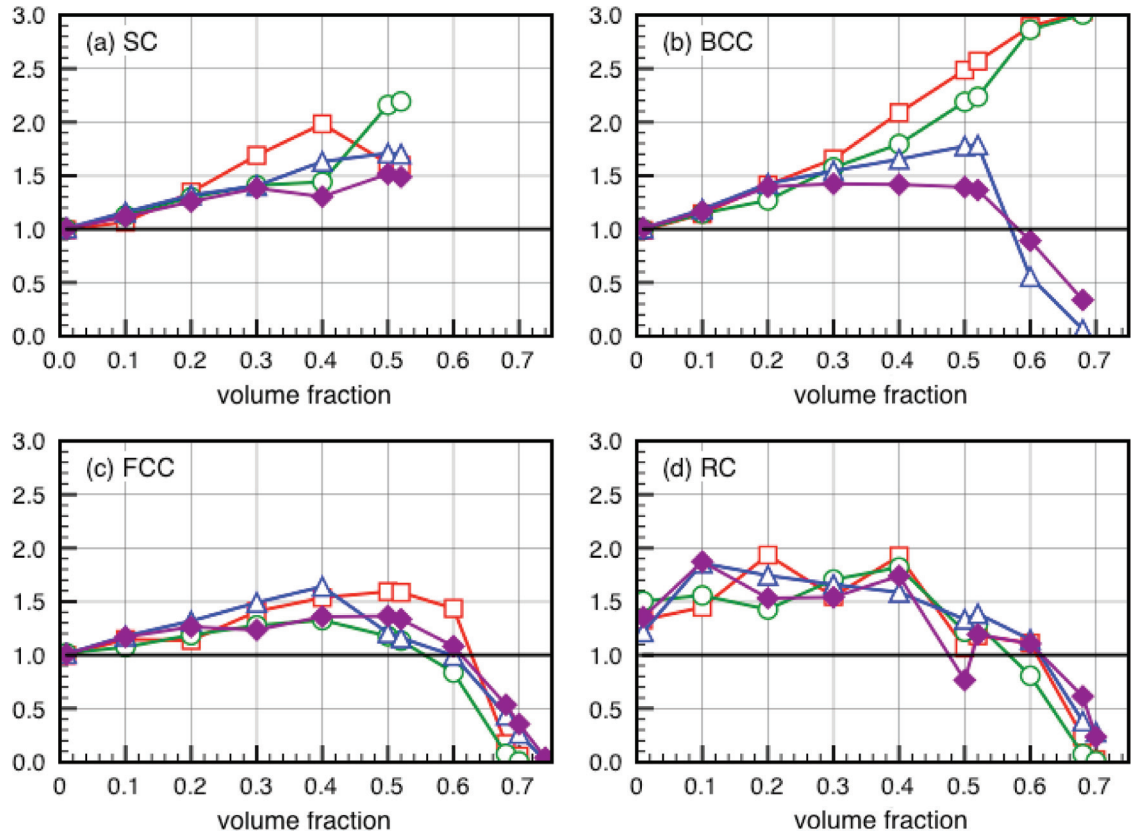

Fig. 1. Permeability ratio of DHD simulations using 2000 (□), 4000 (o), 6000 (Δ), and 10,000 (♦) particles (proposed) relative to the Happel cell model versus volume fraction. Internal geometrical structures are modeled as (a) SC, (b) BCC, (c) FCC, and (d) RC configurations.

simulation method, indicating both DHD simulation and Happel's model converge to the standard permeability form of Eq. (4) at the dilute limit with homogeneous particle distribution. The permeability ratio linearly increases with respect to the volume fraction for the entire volume fraction range, and is consistently greater than 1.0. This implies that the Happel cell model, at least for SC structures, constantly underestimates the permeability; in other words, it overestimates the hydraulic resistance per length. At high volume fractions, close to the SC MPR of 0.524, the permeability ratio exceeds 1.5 for all cases of the particle numbers. Overall, DHD simulations for the SC structure indicate that the applicability of the Happel model is limited to low volume fractions specifically for the SC structure, and its deviation from true depiction of the permeability linearly increases with respect to the volume fraction.

BCC structure. Similarly, the hydraulic permeability of the BCC structure was investigated using the same DHD simulation method for volume fractions as much as the BCC MPR, $\pi\sqrt{3}\,/\,8 = 0.680$. The permeability ratio is shown in Fig. 1(b) with respect to the volume fraction with minor influences from the number of particles at low volume fractions. The permeability ratios monotonically increase from 1.0 within the same region of the SC, i.e., $\phi = [0.01, 0.524]$, in which the Happel model truly underestimates the permeability. However, especially for larger number of particles such as 6,000 and 10,000, the permeability ratios peak near the SC MPR (0.524), start decreasing to below 1.0 at volume fraction around the RLP ratio (0.60), and reach almost zero permeability near the BCC MPR (0.680). The permeability coincidences near the RLP ratio (0.60) between the Happel model and DHD simulations with a larger number of particles are also shown in FCC and RC structures in Figs. 1(c) and (d), respectively (see next sections). A possible reason for the difference in the SC and BCC permeability ratios at high volume fractions can be the distinct structural features observed for a large number of particles. The SC structure intrinsically forms internal straight pores in three directions along which spherical particles are aligned. BCC (as well as FCC) cannot have these straight or less devious pores around the volume fraction of 0.524, above which the permeability ratio declines due to tortuous paths for fluid flow.

FCC structure. Fig. 1(c) shows the permeability ratio of the FCC structure with respect to volume fraction from 0.01 to $\pi\sqrt{2}\,/\,6 = 0.741$ (i.e., the FCC MPR). The influence of the number of particles on the DHD simulations is minimal in this FCC structure compared to the other three structures. Nevertheless, similar trends of the FCC permeability to that of BCC structure is shown in Fig. 1(c), i.e., linearly increasing at low volume fractions up to 1.5, reaching a maximum near the SC MPR (0.524), and decreasing to below the ratio of 1.0 around the RLP ratio (0.60). These results also confirm the general invalidity of the Happel model as indicated in the previous SC and BCC cases. As stated above, monotonic increases of the permeability ratios for small numbers of particles in the BCC case were not observed in this FCC case; however, permeability ratio peaks of FCC structure are observed for all particle numbers, possibly implying that FCC structure is hydraulically more homogeneous.

RC structure. So far we studied the permeability of sphere-packed porous media characterized by the standard SC, BCC and FCC structures. Although such basic solid-state structures provide good insight on how the internal structure of a porous medium influences the hydraulic permeability, in reality, when a colloidal cake layer is formed on the membrane surface, the geometrical configuration can be better characterized by a random packing structure. Overall trends of the permeability ratio for this RC structure with respect to the volume fraction, as shown in Fig. 1(d), are quite similar to those of BCC and FCC. A unique feature of this RC structure is that the permeability ratios are consistently greater than 1.0 even at low volume fractions near 0.1 or below. In SC, BCC, and FCC structures, this ratio commonly converges to 1.0 because the mathematical approach of the Happel model intrinsically assumes complete homogeneity of spherical primary particles. Fig. 1(d) not only indicates that the Happel model underestimates the permeability even at the dilute limit, but also that the porous medium of structural randomness is more permeable than that of geometrical homogeneity at the same volume fraction. This is because locally clumped structures, due to intrinsic randomness, allow fluid to flow through sparser regions, avoiding densely clumped regions of higher resistance. The effect of structural randomness diminishes when the volume fraction reaches the RLP ratio (0.60), near which almost all of the DHD simulation results and the Happel model provide almost identical results, which was the same for all solid-state structures. Similar to other standard structural cases, the permeability ratio near the random close packing (RCP) ratio, 0.64, is around 0.7–0.8. This indicates that the Happel model generally overestimates the hydraulic permeability of the RCP ratio with allowable engineering tolerance.

3.2. Hydrodynamic tortuosity

Because simulation accuracy increases with the number of particles, we used DHD data of 10,000 particles (Fig. 1), and replotted them in Fig. 2(a) to investigate hydraulic tortuosity in terms of internal structures. The local density fluctuation in dilute suspension supersedes effects of homogeneous particle distribution

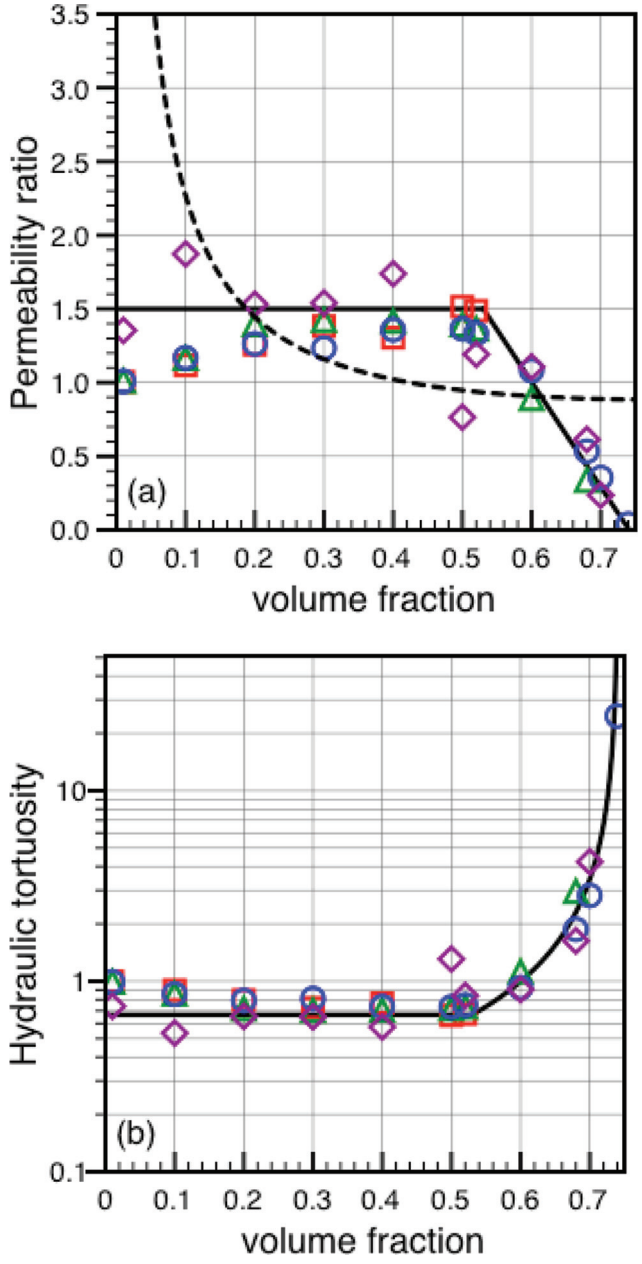

Fig. 2. Plots of (a) permeability ratio of the DHD simulations using SC (□), BCC (Δ), FCC (o), and RC (◇) structures of 10,000 (proposed) particles (symbols), Carman-Kozeny equation (dashed line), and approximate fitting of Eq. (14) (solid line), relative to the Happel cell model, and (b) the hydrodynamic tortuosity as the inverse of the permeability ratio with respect to the volume fraction.

and restricts the validity of Eq. (4), i.e., the permeability expression for the dilute limit pertains only to structured porous media. The permeability ratio of the CK equation to the Happel model indicates that the CK equation is as good as the Happel model, primarily for dense packed structures of volume fraction near 0.5, but erroneously overestimates the permeability at volume fractions less than 0.3.

In this study, the hydraulic tortuosity τ_H is defined as the inverse of the hydraulic permeability that is scaled by the Happel model, and its functional form is derived by fitting data in Fig. 2(a) as

$$\tau_H = \frac{\kappa_{\text{Happel}}}{\kappa_{\text{DHD}}} = \begin{cases} 1 / 1.5 & \text{for} \quad \phi \le 0.524 \\ 0.16 / (0.76 - \phi) & \text{for} \quad \phi \ge 0.524 \end{cases} \tag{14}$$

which implies that the microscopic internal structure of sphere-packed porous media has insignificant influences on the macroscopic hydraulic tortuosity. This structural indifference is similar to that of the diffusive tortuosity $\tau_D = 1 + \frac{1}{2}\phi$ [7,19]. The hydraulic tortuosity τ_H (of the porous media composed of equal-sized spheres) is plotted in Fig. 2(b) as a function of volume fraction ϕ. The nonlinearity of the hydraulic tortuosity begins when the volume fraction is greater than the SC MPR (0.524), below which the hydraulic tortuosity seems to be almost independent of the volume fraction. This is probably because the local clumping induces preferred paths by fluid flow in sparse particle configurations, and this trend continues until the volume fraction approaches the RLP ratio (0.6), above which the hydrodynamic tortuosity drastically increases above 0.667. The reason why hydraulic and diffusive tortuosities have different reference values in the limit of zero volume fraction, i.e., 0.667 and 1.0, is because reference points which permeability and diffusivity are compared to are fluid permeation though a swarm of spheres modelled as a sphere in a tangential-stress-free cell and molecular diffusion in the bulk phase described as 3D random walk, respectively.

4. Conclusions

Random configuration of particles in the dilute limit generates locally heterogeneous structures and therefore promotes uneven fluid flow. This heterogeneity increases the hydraulic permeability by 1.5 times more than the value estimated by conventional theory assuming homogeneous particle distribution. As the volume fraction increases from zero to the SC MPR, the Happel model constantly underestimates the hydraulic permeability. The permeability ratio of the DHD simulations to the Happel model linearly decreases within the volume fractions from 0.524 to 0.741, and only near the RLP ratio of 0.60 do the Happel model and CK equation agree well with the DHD simulation results. Hydraulic tortuosity, defined in this study as the inverse permeability ratio, has a constant value of 2/3 for a wide range of volume fractions from 0.0 to 0.524, above which it drastically increases with volume fraction. Interestingly, structural

influence on the hydraulic permeability appears only in the dilute limit, but it seems insignificant for dense structures of engineering interest.

References

[1] M. Mulder, Basic principles of Membrane Technology, Kluwer Academic Publications, Boston, MA, 1996.

[2] T. Cath, A. Childress and M. Elimelech, Forward osmosis: Principles, applications, and recent developments, J. Membr. Sci., 281 (2006) 70–87.

[3] D.J. Jeffrey and Y. Onishi, Calculation of the resistance and mobility functions for two unequal rigid spheres in low-Reynolds-number flow, J. Fluid Mech., 139 (1984) 261–290.

[4] L. Durlofsky, J.F. Brady and G. Bossis, Dynamic simulation of hydrodynamically interacting particles, J. Fluid Mech., 180 (1987) 21–49.

[5] D.N. Petsev, V.M. Starov and I.B. Ivanov, Concentrated dispersions of charged colloidal particles: sedimentation, ultrafiltration and diffusion, Colloids and Surfaces A, 81 (1993) 65–81.

[6] C. Kittel, Introduction to solid state physics, 1995.

[7] A.S. Kim and H. Chen, Diffusive tortuosity factor of solid and soft cake layers: A random walk simulation approach, J. Membr. Sci., 279 (2006) 129–139.

[8] A.S. Kim and Y. Shi, Dissipative hydrodynamics (DHD) of rigid spherical particles, The American Physical Society, April Meeting, Feb. 13–17, 2010, Washington, DC, USA.

[9] L.S. Blackford, J. Choi, A. Cleary, E.D'Azevedo, J. Demmel, I. Chillon, J. Dongarra, D. Hammarling, G. Henry, A. Petitet, K. Stanley, D. Walker and R.C. Whaley, ScaLAPACK User's Guide, Society for Industrial and Applied Mathematics Philadelphia, PA, 1997.

[10] G.Y. Onoda and E.G. Liniger, Random loose packings of uniform spheres and the dilatancy onset, Phys. Rev. Lett., 64 (1990) 2727–2730.

[11] M.P. Allen and D.J. Tildesley, Computer simulation of liquids, Oxford University Press, Oxford, UK, 1987.

[12] J.F. Brady and G. Bossis, Stokesian Dynamics, Annu. Rev. Fluid Mech., 20 (1988) 111–157.

[13] R. Phillips, J.F. Brady and G. Bossis, Hydrodynamic transport properties of hard-sphere dispersions. I. Suspensions of freely mobile particles, Phys. Fluids, 31 (1988) 3462–3472.

[14] J. Happel, Viscous flow in multiparticle systems: slow motion of fluids relative to beds of spherical particles, AIChE J., 4 (1958) 197–201.

[15] A.S. Kim and K.D. Stolzenbach, The Permeability of Synthetic Fractal Aggregates With Realistic Three-Dimensional Structure, Stolzenbach, J. Colloid Interface Sci., 253 (2002) 315–328.

[16] J. Happel and H. Brenner, Low Reynolds number hydrodynamics, 1991.

[17] H.C. Brinkman, A calculation of the viscosity and the sedimentation velocity for solutions of large chain molecules taking into account the hampered flow of the solvent through each chain molecule, Proc. R. Dutch Acad. Sci, 50 (1947) 618–625.

[18] K.D. Stolzenbach, Scavenging of small particles by fast-sinking porous aggregates, Deep Sea Res., 40 (1993) 359–369.

[19] J.C. Maxwell, Treatise on electricity and magnetism, Dover, New York, 1881.